Table 5
Clinical characteristics of patients in the high and low MPO/GAPDH group

	Total ($n=33$)	High ($n=10$)	Low ($n=23$)	p-Value
Age, Median (range)		34 (27–79)	52 (22–85)	0.0958
PS (0/1/2/3)	5/23/2/3	2/7/1/0	3/16/1/3	0.3445
FAB type				0.0418
M0	2	0	2	
M1	4	4	0	
M2	17	5	12	
M4	8	1	7	
M6	2	0	2	
WBC, median ($\times 10^9\,l^{-1}$)	16.5	58.0	9.9	0.0092
Auer body (present/absent)	14/19	9/1	5/18	0.0003
MPO positivity of blast, median (%)	52	99	34	<0.0001
MLD (present/absent)	15/18	0/10	15/8	0.0005
Cytogenetic risk group				0.0044
Favorable	5	4	1	
Intermediate	20	6	14	
Adverse	7	0	7	
Not done	1	0	1	

MLD, multilineage dysplasia.

were positive for AC133 antigen on the surface. In this study, we measured the amount of MPO transcripts in AC133 positive leukemia cells. As shown in cases with t(8;21), the expression of AML1-ETO fusion transcripts was detectable after positive selection with an AC133-column, demonstrating these four purified samples, at least, contained leukemia cells. Morphological examination showed that the selected cells did not contain any promyelocytes or more mature cells.

The expression of the MPO gene in AML cells was previously reported by several groups [28–30]. Zaki et al. used Northern blot analysis to examine the expression of MPO mRNA in 32 AML samples, and they found that M3 cases had the highest level of expression followed by M2, M4, M1 and M5 cases [28]. Since their results reflected the myeloid differentiation of leukemia cells defined by the FAB subtypes, it seemed that the AML samples they tested (MNC samples, >80% blasts) contained a differentiated fraction of leukemia cells. In our present study, AML with maturation, such as M2 and M4 cases were found in both MPOg-H and MPOg-L groups, showing a clear contrast to the report from Zaki et al. We assume that the amount of MPO mRNA in AC133 positive leukemia cells did not clearly relate to the FAB subgroup of AML defined by the morphological differentiation of leukemia cells.

It has been shown that genes expressed in immature hamatopoietic cells including stem cells do not always represent the lineage commitment [31,32]. Using genetically engineered mice, Ye et al. demonstrated that one of the myeloid specific genes, lysozyme, was expressed in bone marrow cells that have potential to reconstitute both myeloid and lymphoid cells [33]. We do not have any clear answer whether the expression of the MPO gene in AC133 positive leukemia cells was independent of myeloid commitment or it was a part of myeloid differentiation of these cells. The fact that some cells in cases belonging to MPOg-H also expressed MPO protein and its enzymatic activity suggested, at least in these cases, that MPO expression represented the early process of myeloid commitment and/or maturation before apparent morphological differentiation.

Comparing to the MPOg-L, belonging to the MPOg-H group was significantly related to the better survival. Some clinical features repeatedly observed in favorable AML cases were found among cases in the MPOg-H group: all cases with t(8;21) and no cases with adverse karyotypes or MLD were in this group [34]. These data supported the difference in survival between these two groups. We previously demonstrated that the percentage of MPO positive blasts was an independent prognostic factor for AML [8]. However, there was no significant difference in overall survival by the percentage of MPO positive blasts in this study ($p=0.100$), but by the level of the MPO gene in AC133 positive fraction. It might be because of the small number of cases, or it was because the level of the MPO gene in AC133 positive fraction might have a stronger impact on the survival of patients with AML. Survival curve of Group II (high percentage of MPO positive blasts but low MPO/GAPDH ratio) was similar to that of Group III in this series (data not shown). This point needs to be confirmed with a larger number of cases.

In summary, we confirmed that MLD phenotype was significantly related to the low expression of the MPO gene in AC133 positive cells. We also demonstrated the possible prognostic value of the MPOg-H group in overall survival associated with positive relation to the karyotype, t(8;21) and the negative relation to the adverse karyotypes. It is necessary to investigate whether several factors seen in favorable AML cases, such as karyotype and MPO expression have biological relationship at the molecular level.

Acknowledgements

This work was supported in part by grant from the Ministry of Education, Culture, Sports, Science and Technology (Y.M., H.M. and M.T.), and the Ministry of Health, Labour and Welfare of Japan (Y.M.). We thank A. Mizugashira-Kubota and E. Yamazoe for their assistance.

J. Taguchi, Y. Sawayama, K. Ando and C. Tsutsumi worked on the experiments with advices from H. Tsushima. S. Yoshida, T. Fukushima and I. Jinnai collected clinical samples and data, and T. Hata and K. Kuriyama were in charge of the diagnosis. S. Honda performed statistical analyses. Y. Miyazaki organized this project and wrote the paper under the supervision of H. Mano and M. Tomonaga.

References

[1] Babior BM. Oxygen-dependent microbial killing by phagocytes (first of two parts). N Engl J Med 1978;298:659–68.
[2] Babior BM. Oxygen-dependent microbial killing by phagocytes (second of two parts). N Engl J Med 1978;298:721–5.
[3] Koeffler HP, Ranyard J, Pertcheck M. Myeloperoxidase: its structure and expression during myeloid differentiation. Blood 1985;65:484–91.
[4] Winterbourn CC, Vissers MC, Kettle AJ. Myeloperoxidase. Curr Opin Hematol 2000;7:53–8.
[5] Bennett JM, Catovsky D, Daniel MT, Flandrin G, Galton DA, Gralnick HR, et al. Proposed revised criteria for the classification of acute myeloid leukaemia. A report of the French–American–British Cooperative Group. Ann Intern Med 1985;103:620–9.
[6] Hoyle CF, Gray RG, Wheatley K, Swirsky D, de Bastos M, Sherrington P, et al. Prognostic importance of Sudan Black positivity: a study of bone marrow slides from 1386 patients with de novo acute myeloid leukaemia. Br J Haematol 1991;79:398–407.
[7] Matsuo T, Cox C, Bennett JM. Prognostic significance of myeloperoxidase positivity of blast cells in acute myeloblastic leukemia without maturation (FAB: M1): an ECOG study. Hematol Pathol 1989;3:153–8.
[8] Matsuo T, Kuriyama K, Miyazaki Y, Yoshida S, Tomonaga M, Emi N, et al. The percentage of myeloperoxidase-positive blast cells is a strong independent prognostic factor in acute myeloid leukemia, even in the patients with normal karyotype. Leukemia 2003;17:1538–43.
[9] Yin AH, Miraglia S, Zanjani ED, Almeida-Porada G, Ogawa M, Leary AG, et al. AC133, a novel marker for human hematopoietic stem and progenitor cells. Blood 1997;90:5002–12.
[10] Miraglia S, Godfrey W, Yin AH, Atkins K, Warnke R, Holden JT, et al. A novel five-transmembrane hematopoietic stem cell antigen: isolation, characterization, and molecular cloning. Blood 1997;90:5013–21.
[11] Bonnet D, Dick JE. Human acute myeloid leukemia is organized as a hierarchy that originates from a primitive hematopoietic cell. Nat Med 1997;3:730–7.
[12] de Wynter EA, Buck D, Hart C, Heywood R, Coutinho LH, Clayton A, et al. CD34+ AC133+ cells isolated from cord blood are highly enriched in long-term culture-initiating cells, NOD/SCID-repopulating cells and dendritic cell progenitors. Stem Cells 1998;16:387–96.
[13] Bhatia M, Bonnet D, Murdoch B, Gan OI, Dick JE. A newly discovered class of human hematopoietic cells with SCID-repopulating activity. Nat Med 1998;4:1038–45.
[14] Gallacher L, Murdoch B, Wu DM, Karanu FN, Keeney M, Bhatia M. Isolation and characterization of human CD34(−)Lin(−) and CD34(+)Lin(−) hematopoietic stem cells using cell surface markers AC133 and CD7. Blood 2000;95:2813–20.
[15] Shmelkov SV, Jun L, St Clair R, McGarrigie D, Derderian CA, Usenko JK, et al. Alternative promoters regulate transcription of the gene that encodes stem cell surface protein AC133. Blood 2004;103:2055–61.
[16] Ohmine K, Ota J, Ueda M, Ueno S, Yoshida K, Yamashita Y, et al. Characterization of stage progression in chronic myeloid leukemia by DNA microarray with purified hematopoietic stem cells. Oncogene 2001;20:8249–57.
[17] Qian Z, Fernald AA, Godley LA, Larson RA, Le Beau MM. Expression profiling of CD34+ hematopoietic stem/progenitor cells reveals distinct subtypes of therapy-related acute myeloid leukaemia. Proc Natl Acad Sci USA 2002;99:14925–30.
[18] Tsutsumi C, Ueda M, Miyazaki Y, Yamashita Y, Choi YL, Ota J, et al. DNA microarray analysis of dysplastic morphology associated with acute myeloid leukemia. Exp Hematol 2004;32:828–35.
[19] Kuriyama K, Tomonaga M, Matsuo T, Kobayashi T, Miwa H, Shirakawa S, et al., Japan Adult Leukaemia Study Group (JALSG). Poor response to intensive chemotherapy in de novo acute myeloid leukaemia with trilineage myelodysplasia. Br J Haematol 1994;86:767–73.
[20] Gabert J, Beillard E, van der Velden VHJ, Bi W, Grimwade D, Pallisgaard N, et al. Standardization and quality control studies of 'real-time' quantitative reverse transcriptase polymerase chain reaction of fusion gene transcripts for residual disease detection in leukaemia—A Europe Against Cancer Program. Luekemia 2003;17:2318–57.
[21] Shibata A, Bennett JM, Castoldi GL, Catovsky D, Flandrin G, Jaffe ES, et al. Recommended methods for cytological procedures in haematology. International Committee for Standardization in Haematology (ICSH). Clin Lab Haematol 1985;7:55–74.
[22] Grimwade D, Walker H, Oliver F, Wheatley K, Harrison C, Harrison G, et al. The importance of diagnostic cytogenetics on outcome in AML: analysis of 1612 patients entered into the MRC AML 10 trial. The Medical Research Council Adult and Children's Leukaemia Working Parties. Blood 1998;92:2322–33.
[23] Miyazaki Y, Kuriyama K, Miyawaki S, Ohtake S, Sakamaki H, Matsuo T, et al. Cytogenetic heterogeneity of acute myeloid leukaemia (AML) with trilineage dysplasia: Japan Adult Leukaemia Study Group-AML 92 study. Br J Haematol 2003;120:56–62.
[24] Vercauteren SM, Sutherland HJ. CD133 (AC133) expression on AML cells and progenitors. Cytotherapy 2001;3:449–59.
[25] Fauth F, Weidmann E, Martin H, Schneider B, Sonnhoff S, Hoelzer D. AC133 expression on acute myeloid leukemia blasts: correlation to FAB and to CD34 expression and possible implications for peripheral blood progenitor cell purging in AML. Leuk Res 2001;25:191–6.
[26] Kuci S, Wessels JT, Buhring HJ, Schilbach K, Schumm M, Seitz G, et al. Identification of a novel class of human adherent CD34-stem cells that give rise to SCID-repopulating cells. Blood 2003;101:869–76.
[27] Koehl U, Zimmermann S, Esser R, Sorensen J, Gruttner HP, Duchscherer M, et al. Autologous transplantation of CD133 selected hematopoietic progenitor cells in a pediatric patient with relapsed leukemia. Bone Marrow Transplant 2002;29:927–30.
[28] Zaki SR, Austin GE, Swan D, Srinivasan A, Ragab AH, Chan WC. Human myeloperoxidase gene expression in acute leukemia. Blood 1989;74:2096–102.
[29] Chang KS, Trujillo JM, Cook RG, Stass SA. Human myeloperoxidase gene: molecular cloning and expression in leukemic cells. Blood 1986;68:1411–4.
[30] Austin GE, Chan WC, Zhao W, Racine M. Myeloperoxidase gene expression in normal granulopoiesis and acute leukemias. Leuk Lymphoma 1994;15:209–20.
[31] Hu M, Krause D, Greaves M, Sharkis S, Dexter M, Heyworth C, et al. Multilineage gene expression precedes commitment in the hemopoietic system. Genes Dev 1997;11:774–85.

[32] Akashi K, Traver D, Miyamoto T, Weissman IL. A clonogenic common myeloid progenitor that gives rise to all myeloid lineages. Nature 2000;404:193–7.
[33] Ye M, Iwasaki H, Laiosa CV, Stadtfeld M, Xie H, Heck S, et al. Hematopoietic stem cells expressing the myeloid lysozyme gene retain long-term, multilineage repopulation potential. Immunity 2003;19:689–99.
[34] Lowenberg B, Downing JR, Burnett A. Acute myeloid leukemia. N Engl J Med 1999;341:1051–62.

Oncogene (2006) 25, 139–146

www.nature.com/onc

SHORT COMMUNICATION

Epigenetic silencing of *AXIN2* in colorectal carcinoma with microsatellite instability

K Koinuma[1,2], Y Yamashita[1], W Liu[3], H Hatanaka[1], K Kurashina[1,2], T Wada[1], S Takada[1], R Kaneda[1], YL Choi[1], S-I Fujiwara[1], Y Miyakura[2], H Nagai[2] and H Mano[1,4]

[1]Division of Functional Genomics, Jichi Medical School, Tochigi, Japan; [2]Department of Surgery, Jichi Medical School, Tochigi, Japan; [3]Division of Experimental Pathology, Mayo Clinic and Mayo Medical School, Rochester, MN, USA and [4]CREST, Japan Science and Technology Agency, Saitama, Japan

Mutation or epigenetic silencing of mismatch repair genes, such as *MLH1* and *MSH2*, results in microsatellite instability (MSI) in the genome of a subset of colorectal carcinomas (CRCs). However, little is yet known of genes that directly contribute to tumor formation in such cancers. To characterize MSI-dependent changes in gene expression, we have now compared transcriptomes between fresh CRC specimens positive or negative for MSI ($n = 10$ for each) with the use of high-density oligonucleotide microarrays harboring > 44 000 probe sets. Correspondence analysis of the expression patterns of isolated MSI-associated genes revealed that the transcriptome of MSI$^+$ CRCs is clearly distinct from that of MSI$^-$ CRCs. Such MSI-associated genes included that for AXIN2, an important component of the WNT signaling pathway. *AXIN2* was silenced, apparently as a result of extensive methylation of its promoter region, specifically in MSI$^+$ CRC specimens. Forced expression of *AXIN2*, either by treatment with 5′-azacytidine or by transfection with *AXIN2* cDNA, resulted in rapid cell death in an MSI$^+$ CRC cell line. These data indicate that epigenetic silencing of *AXIN2* is specifically associated with carcinogenesis in MSI$^+$ CRCs.

Oncogene (2006) **25,** 139–146. doi:10.1038/sj.onc.1209009; published online 10 October 2005

Keywords: epigenetics; colorectal carcinoma; microsatellite instability; AXIN2; MLH1

Colorectal carcinoma (CRC) is one of the leading causes of cancer death in humans. Evidence indicates the existence of two major types of genomic instability in CRCs: chromosomal instability and microsatellite instability (MSI) (Lengauer *et al.*, 1998). Whereas chromosomal instability is associated with an abnormal DNA content (such as aneuploidy), inactivation of the tumor suppressor gene *TP53*, and activation of oncogenes (Kinzler and Vogelstein, 1996), MSI is associated with defects in DNA mismatch repair (MMR) that result in frameshift mutations in microsatellite repeats and thereby affect the structure of genes containing such repeats (Ionov *et al.*, 1993).

Although germline mutations of MMR genes have been detected in the genome of individuals with hereditary nonpolyposis colorectal cancer (Fishel *et al.*, 1993; Bronner *et al.*, 1994; Papadopoulos *et al.*, 1994), many sporadic CRCs positive for MSI are associated with epigenetic silencing of nonmutated MMR genes (Toyota *et al.*, 1999; Miyakura *et al.*, 2001). MSI$^+$ CRCs are characterized by specific clinicopathologic features and gene mutations. They occur with a higher frequency in women than in men, develop in the right side of the colon, and manifest a mucinous or poorly differentiated histopathology. Many of the CpG dinucleotides within the promoter region of the MMR gene *MLH1* are methylated (Cunningham *et al.*, 1998; Veigl *et al.*, 1998) and the *BRAF* gene frequently contains activating mutations (Koinuma *et al.*, 2004) in MSI$^+$ CRCs. Multiple genomic fragments have been found to be methylated in such CRCs (Toyota *et al.*, 1999), and an entity of CRC with a CpG island methylator phenotype has been proposed (Issa, 2004). The repertoire of genes that become methylated specifically in CRCs positive for *MLH1* methylation has remained uncharacterized, however.

To characterize directly the transcriptome specifically associated with MSI$^+$ CRC, we have now compared transcriptomes between fresh CRC specimens with or without MSI. Unexpectedly, we found that the expression of *AXIN2*, which encodes a component of the WNT signaling pathway, was markedly suppressed among the former tumors. CpG sequences within the *AXIN2* promoter were revealed to be extensively methylated in such CRCs. Forced expression of *AXIN2* inhibited cell proliferation in an MSI$^+$ CRC cell line, indicating that loss of *AXIN2* transcription is directly associated with carcinogenesis in MSI$^+$ CRCs.

To identify genes whose expression is specifically altered in MSI$^+$ CRCs, we first compared the transcriptomes of CRCs with or without MSI. A total of 248 consecutive cases of CRC were examined for MSI status

Correspondence: Professor H Mano, Division of Functional Genomics, Jichi Medical School, 3311-1 Yakushiji, Kawachigun, Tochigi 329-0498, Japan.
E-mail: hmano@jichi.ac.jp
Received 28 April 2005; revised 7 July 2005; accepted 13 July 2005; published online 10 October 2005

as well as for methylation of the promoter region of *MLH1* (Koinuma *et al.*, 2004). Most ($n=213$) of the cancer specimens were MSI$^-$, with the remainder ($n=35$) being positive for MSI. To compare the transcriptomes of these two subtypes of CRC, we randomly selected 10 specimens from each group and subjected them to gene expression profiling with microarrays (Affymetrix GeneChip HGU133) that harbor >44 000 probe sets. The clinical characteristics of the patients whose CRC specimens were subjected to microarray analysis are summarized in Table 1.

To exclude transcriptionally silent genes from our analyses, we first chose probe sets that received the 'Present' call from Microarray Suite 5.0 (Affymetrix) in at least 10% ($n=2$) of the samples. Two-way hierarchical clustering (Alon *et al.*, 1999) of the 20 patients based on the expression profiles of the isolated 21 888 probe sets failed to separate those with MSI$^+$ CRC from those with MSI$^-$ CRC (data not shown). We therefore attempted to identify 'MSI-associated probe sets' whose expression intensities differed significantly (Student's *t*-test, $P<0.001$) between the two classes and whose effect size (absolute difference in mean expression level) was $\geqslant 50$ U. Two-way clustering analysis with the 24 probe sets that fulfilled both these criteria clearly separated the individuals of the two clinical classes (Figure 1a). The distinct transcriptomes of the two classes were also confirmed by correspondence analysis (Fellenberg *et al.*, 2001), which reduced the complexity of the gene expression patterns from 24 to three dimensions. Projection of the study subjects into a virtual three-dimensional space based on their calculated coordinates revealed that the MSI$^+$ specimens were positioned apart from the MSI$^-$ ones (Figure 1b). These data indicate that the two classes of CRC possess distinct gene expression profiles, or 'molecular signatures', and they also suggest the feasibility of gene expression-based differential diagnosis of the two CRC subtypes.

Table 1 Clinical characteristics of the study subjects enrolled in microarray analysis

Patient ID	*Age (years)*	*Sex*	*MSI status*	MLH1 *methylation*	BRAF *gene*	KRAS2 *gene*	*Tumor site*	*Dukes stage*	*Pathology*	AXIN2 *methylation*
225	83	Female	Positive	Yes	Mutant	Wild	Proximal	C	Well	Yes
263	86	Female	Positive	Yes	Mutant	Wild	Proximal	C	Mod	Yes
280	83	Female	Positive	Yes	Mutant	Wild	Proximal	C	Well	Yes
305	74	Male	Positive	Yes	Mutant	Wild	Proximal	B	Sig	No
318	76	Female	Positive	Yes	Mutant	Wild	Proximal	B	Well	Yes
336	68	Male	Positive	Yes	Mutant	Wild	Proximal	B	Muc	No
413	69	Female	Positive	Yes	Mutant	Wild	Proximal	A	Well	No
416	76	Female	Positive	Yes	Mutant	Wild	Proximal	B	Muc	No
433	54	Female	Positive	Yes	Wild	Wild	Proximal	D	Well	Yes
479	74	Female	Positive	Yes	Mutant	Wild	Proximal	B	Mod	No
238	74	Male	Negative	No	Wild	Mutant	Distal	A	Well	No
249	62	Male	Negative	No	Wild	Wild	Proximal	B	Well	No
278	73	Male	Negative	No	Wild	Wild	Proximal	C	Well	No
295	71	Female	Negative	No	Wild	Mutant	Proximal	C	Well	No
298	70	Male	Negative	No	Wild	Mutant	Proximal	D	Well	No
307	80	Female	Negative	No	Wild	Wild	Proximal	C	Mod	No
308	62	Male	Negative	No	Wild	Wild	Distal	B	Mod	No
319	53	Female	Negative	No	Wild	Wild	Distal	A	Well	No
419	45	Female	Negative	No	Wild	Mutant	Proximal	D	Muc	No
426	42	Female	Negative	No	Wild	Wild	Proximal	C	Well	No

Well = well-differentiated adenocarcinoma; Mod = moderately differentiated adenocarcinoma; Sig = signet ring cell adenocarcinoma; Muc = mucinous adenocarcinoma. Methylation of *AXIN2* promoter region was determined by COBRA method.

Figure 1 Comparison of transcriptomes between CRCs positive or negative for MSI. (**a**) Subject tree generated by two-way clustering analysis with 24 probe sets that contrasted the two clinical conditions ($P<0.001$; effect size, $\geqslant 50$ U). Tumor samples were obtained from individuals with sporadic CRC who underwent surgical treatment at Jichi Medical School Hospital. Written informed consent was obtained from all patients, and the present study was approved by the ethics committee of Jichi Medical School. Microsatellite stability was determined by analysis of nine microsatellite repeat loci (three dinucleotide repeats and six mononucleotide repeats) as described previously (Miyakura *et al.*, 2001), and MSI status was stratified according to the criteria of the National Cancer Institute workshop (Boland *et al.*, 1998). Total RNA was extracted from ~100 mg of tissue, and was used in the hybridization experiments with GeneChip HGU133 A&B microarrays (Affymetrix), which harbor >44 000 probe sets corresponding to ~33 000 human genes, as described previously (Ohki-Kaneda *et al.*, 2004). The mean expression intensity of the internal positive control probe sets (http://www.affymetrix.com/support/technical/mask_files.affx) on the microarrays was set to 500 units (U) in each hybridization, and the fluorescence intensity of each probe set was normalized accordingly. All normalized array data are available at the Gene Expression Omnibus website (http://www.ncbi.nlm.nih.gov/geo) under the Accession Number GSE2138. Each column corresponds to a separate sample (MSI$^-$, green; MSI$^+$, red), and each row to a probe set whose expression is color-coded according to the indicated scale. Gene symbols are shown on the right; 225541_at, 226545_at, and 242414_at are expressed sequence tag IDs designated by Affymetrix (http://www.affymetrix.com). Annotations and expression intensities for the probe sets are presented in Supplementary Table 1. Note that *MLH1* expression was specifically suppressed in the MSI$^+$ samples. (**b**) Samples were projected into a virtual space with coordinates calculated by correspondence analysis of the 24 probe sets shown in (**a**). Correspondence analysis was performed with ViSta software (http://www.visualstats.org) for all genes showing a significant difference.

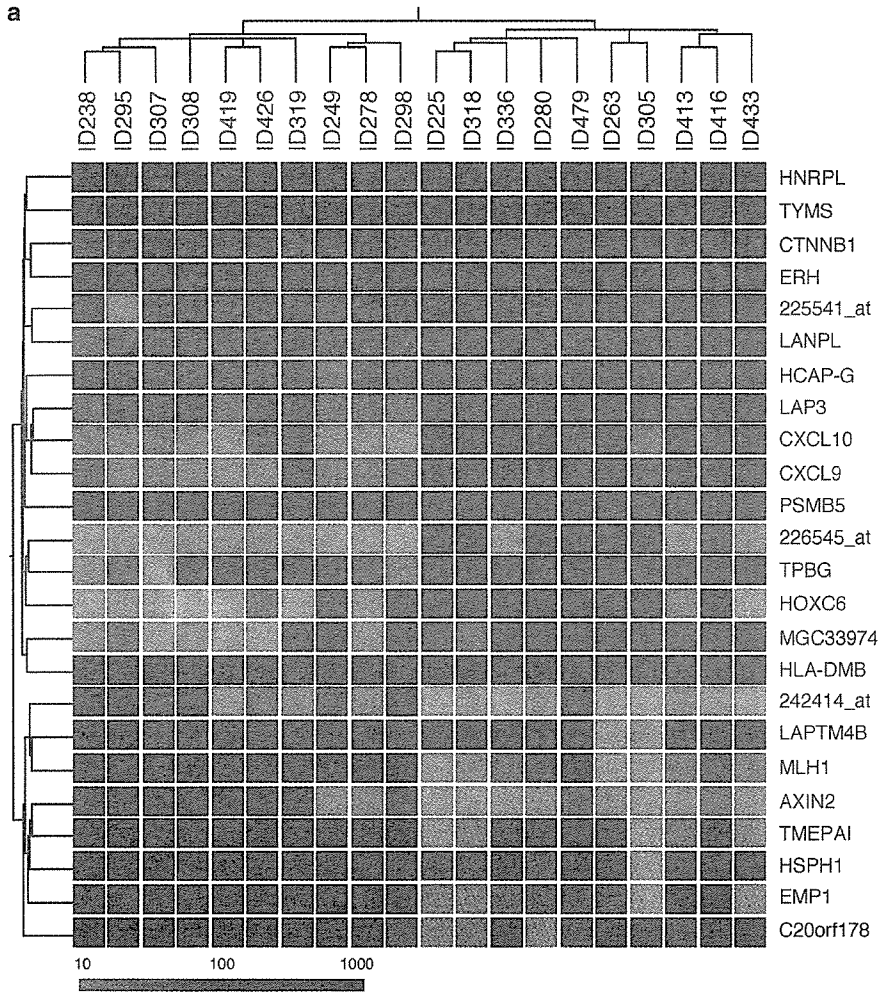
a
ID238
ID295
ID307
ID308
ID419
ID426
ID319
ID249
ID278
ID298
ID225
ID318
ID336
ID280
ID479
ID263
ID305
ID413
ID416
ID433
HNRPL
TYMS
CTNNB1
ERH
225541_at
LANPL
HCAP-G
LAP3
CXCL10
CXCL9
PSMB5
226545_at
TPBG
HOXC6
MGC33974
HLA-DMB
242414_at
LAPTM4B
MLH1
AXIN2
TMEPAI
HSPH1
EMP1
C20orf178
10
100
1000

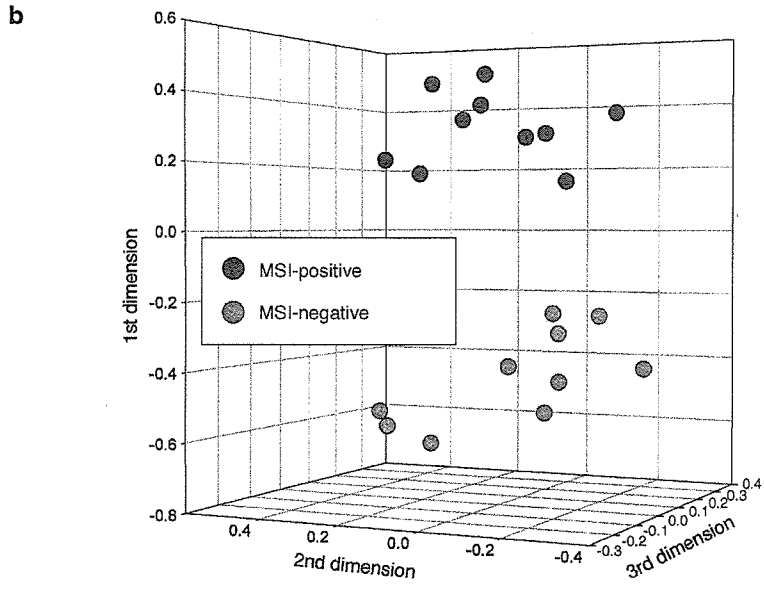
b
1st dimension
2nd dimension
3rd dimension
MSI-positive
MSI-negative

The isolated MSI-associated genes include *AXIN2* and *CTNNB1* (β-catenin), both of which encode key participants in the WNT signaling pathway (Tolwinski and Wieschaus, 2004). Dysregulation of ubiquitin-dependent degradation of β-catenin contributes to carcinogenesis in a variety of CRCs and hepatocellular carcinomas (Narayan and Roy, 2003). AXIN2, similar to AXIN1, functions as a scaffold protein to facilitate this ubiquitination process by recruiting adenomatous polyposis coli (APC), glycogen synthase kinase-3β, and β-catenin (Behrens *et al.*, 1998). Defects in the degradation of β-catenin have been shown to result from mutations in *AXIN1*, *AXIN2*, *APC*, or *CTNNB1* (Rubinfeld *et al.*, 1997; Liu *et al.*, 2000; Satoh *et al.*, 2000; Smith *et al.*, 2002). Our data therefore suggest that transcriptional suppression of *AXIN2* might represent a novel mechanism by which the function of the APC-AXIN–β-catenin complex is impaired in CRC.

To confirm the MSI-associated change in *AXIN2* expression, we measured the abundance of the corresponding mRNA in the original 20 study specimens by quantitative reverse transcription–polymerase chain reaction (RT–PCR) analysis (Figure 2a). Comparison of the amount of *AXIN2* mRNA determined by RT–PCR with that determined by microarray analysis yielded a Pearson's correlation coefficient (r) of 0.89, indicating that the two data sets were highly correlated ($P<0.001$). (Also see Supplementary Figure 1 for verification of microarray data by RT–PCR.)

With the use of RT–PCR, we then measured the amount of *AXIN2* mRNA in a larger number of samples (seven additional specimens of MSI$^+$ CRC, for a total of 17; 10 additional specimens of MSI$^-$ CRC, for a total of 20; three MSI$^+$ CRC cell lines; two MSI$^-$ CRC cell lines). The abundance of *AXIN2* transcripts in most of the MSI$^+$ CRC specimens and cell lines was reduced compared with that in the MSI$^-$ ones (Figure 2b); an *AXIN2*/*ACTB* transcript ratio of $<5\times10^{-4}$ was apparent in 13 of the 17 MSI$^+$ CRC specimens, but in only five of the 20 MSI$^-$ ones (Fisher's exact probability test, $P=0.003$). Importantly, a similar MSI-dependent suppression of *AXIN1* expression was not observed among these specimens ($P=0.31$) (data not shown).

Human *AXIN2* possesses a relatively large CpG island within its promoter region (nucleotide positions, chr17: 60986365–60987824). We therefore examined the methylation status of the CpG sites within this region by nucleotide sequencing after sodium bisulfite treatment. Extensive methylation of the CpG island in the *AXIN2* promoter was apparent in CRC specimens positive for MSI and for the loss of *AXIN2* expression (Figure 2c). The promoter region in the MSI$^+$ CRC cell line HCT116 (Wheeler *et al.*, 1999) was also heavily methylated. The *MLH1* promoter in HCT116 cells is not methylated, but the coding sequence of the gene contains a mutation that results in MSI (Wheeler *et al.*, 1999).

On the basis of these findings, we examined the methylation status of the *AXIN2* promoter in 37 clinical specimens and five cell lines by combined bisulfite restriction analysis (COBRA) (Xiong and Laird, 1997). CpG methylation was detected in five of the 17 MSI$^+$ specimens, but in none of the 20 MSI$^-$ specimens (Table 1; see Supplementary Table 2). Methylation of the *AXIN2* promoter was not detected in normal colon tissue obtained from the individuals with MSI$^+$ CRC (data not shown), suggesting that *AXIN2* methylation was a somatic event in these patients.

We then tested whether the amount of the encoded protein correlated with that of *AXIN2* mRNA in CRC specimens (Figure 2d). Immunohistochemical staining showed that AXIN2 was abundant in a specimen with a high mRNA content (ID308), but was present in much smaller amounts in two specimens with a low mRNA content (ID263, ID295). Although a large amount of *AXIN2* mRNA was not always associated with a large amount of protein, a small amount of mRNA was consistently associated with a small amount of protein (data not shown).

To examine directly whether epigenetic silencing of *AXIN2* is relevant to the change in the growth properties of CRC cells, we restored *AXIN2* expression, either by 5′-azacytidine treatment or by introduction of *AXIN2* cDNA, in an MSI$^+$ CRC cell line. 5′-Azacytidine inhibits *de novo* methylation of genomic DNA and thereby induces demethylation of the genome of proliferating cells (Christman, 2002). HCT116 cells were incubated for 3 days with various concentrations of 5′-azacytidine and were then subjected to COBRA for determination of the methylation status of the *AXIN2* promoter. Treatment with 5′-azacytidine reduced the level of methylation of the *AXIN2* promoter in a concentration-dependent manner (Figure 3a). This effect of 5′-azacytidine was accompanied by an increase in the amount of *AXIN2* mRNA in the cells (Figure 3b) as well as by the induction of cell death (Figure 3c).

Given that 5′-azacytidine likely affects the transcription of other genes in addition to that of *AXIN2*, the growth inhibitory effect observed in HCT116 cells might not have been attributable solely to the induction of *AXIN2* expression. To examine the direct effect of *AXIN2*, we introduced its cDNA into HCT116 cells by transfection. However, an introduction of *AXIN2* cDNA (even with the use of an inducible system) resulted in rapid cell death, and we could not establish stable transformants of cell lines with such expression constructs (data not shown). Therefore, we generated an amphotropic recombinant retrovirus that confers simultaneous expression of both an MYC epitope-tagged form of AXIN2 and mouse CD8. Human kidney 293 cells infected with this virus, but not those infected with a mock virus, expressed AXIN2 (Figure 3d). HCT116 cells were then infected with the virus and were subjected to affinity chromatography 48 h thereafter to isolate cells that express CD8. Given that CD8-expressing cells would be expected also to express AXIN2, this column purification step should result in rapid enrichment of AXIN2-expressing cells. The isolated cells indeed contained a substantial amount of *AXIN2* mRNA as revealed by RT–PCR (Figure 3e). The purified CD8$^+$ HCT116 cells were then cultured for 3 days to characterize their growth properties. Forced expression of AXIN2 resulted in marked inhibition of cell growth

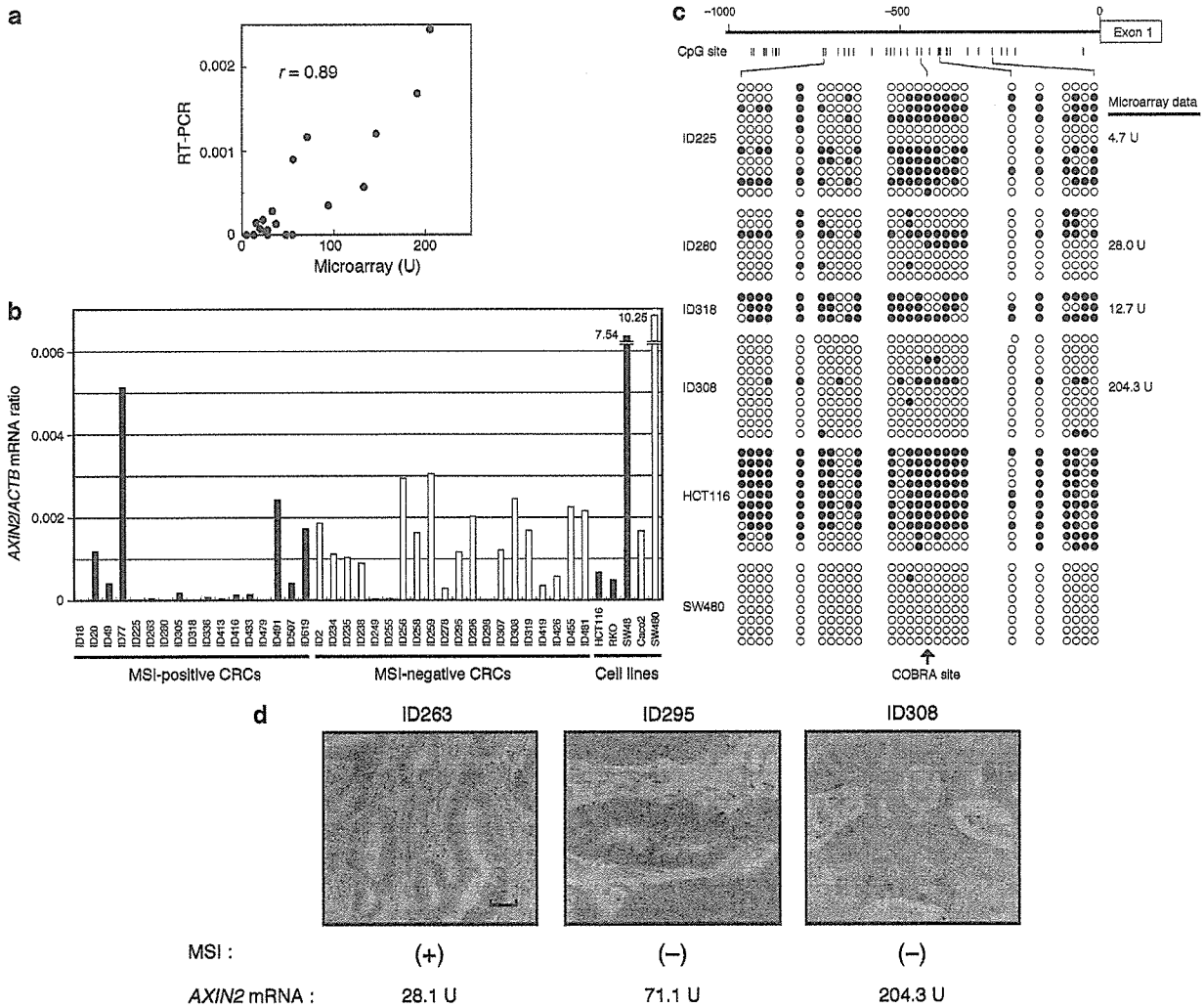

Figure 2 Suppression of *AXIN2* expression in CRCs positive for MSI. (**a**) Comparison of the abundance of *AXIN2* mRNA in study specimens as determined by microarray and RT–PCR analyses. For the latter, the amount of *AXIN2* mRNA was expressed relative to that of *ACTB* mRNA. Pearson's correlation coefficient (*r*) for the comparison is indicated. Portions of double-stranded cDNA were subjected to PCR with a QuantiTect SYBR Green PCR Kit (Qiagen). The amplification protocol comprised incubations at 94°C for 15 s, 63°C for 30 s, and 72°C for 60 s. Incorporation of the SYBR Green dye into PCR products was monitored in real time with an ABI PRISM 7700 sequence detection system (PE Applied Biosystems), thereby allowing determination of the threshold cycle (C_T) at which exponential amplification of products begins. The amount of target cDNAs relative to that of the β-actin (*ACTB*) cDNA was calculated from the C_T values with the use of Sequence Detector ver. 1.6.3 software (PE Applied Biosystems). The primers used for PCR amplification were 5′-CTGGCTCCAGAAGATCACAAAG-3′ and 5′-ATCTCCTCAAACACCGCTCCA-3′ for *AXIN2* and 5′-CCATCATGAAGTGTGACGTGG-3′ and 5′-GTCCGCCTAGAAGCATTTGCG-3′ for *ACTB*. (**b**) Comparison of the amount of *AXIN2* mRNA relative to that of *ACTB* mRNA (as determined by RT–PCR) between MSI^+ (closed bars) and MSI^- (open bars) CRC specimens and cell lines. (**c**) Genomic DNA of the indicated clinical specimens and CRC cell lines was treated with sodium bisulfite (Koinuma *et al*., 2004), after which the *AXIN2* promoter region was amplified by PCR with the primers 5′-TTGTATATAGTTTA GYGGTTGGG-3′ and 5′-AAATCTAAACTCCCTACACACTT-3′. Closed and open circles indicate methylated and unmethylated CpG sites, respectively. The positions of the CpG sites are indicated at the top, the *Hha*I digestion site for COBRA is indicated by the arrow, and the microarray data for *AXIN2* expression are shown on the right. (**d**) Immunohistochemical analysis of the indicated clinical specimens with antibodies to AXIN2. The MSI status and the expression level of *AXIN2* determined by microarray analysis are indicated. Immunohistochemical analysis of AXIN2 expression was performed as described previously (Leung *et al*., 2002). Sections (5 μm) of formalin-fixed, paraffin-embedded tissue were mounted on Probe-On slides (Fisher Scientific), which were then incubated first for 1 h at room temperature with 1.5% normal horse serum and then overnight at 4°C with goat polyclonal antibodies to AXIN2 (Santa Cruz Biotechnology). Immune complexes were detected by the avidin–biotin–peroxidase method with 3,3′-diaminobenzidine as the chromogenic substrate (Vectastain ABC kit, Vector Laboratories). The sections were counterstained with hematoxylin. Scale bar, 50 μm.

(Figure 3f), indicating that silencing of *AXIN2* is indeed relevant to tumorigenesis. We also examined if the expression of *AXIN2* directly suppresses the WNT signaling pathway. For this purpose, we utilized a luciferase-based reporter plasmid (TOPflash) for the T-cell factor (TCF) activity, which is a direct target of

β-catenin (Korinek *et al*., 1997). As shown in Figure 3g, a forced expression of *AXIN2* induced a marked suppression in the luciferase activity in HCT116 cells. On the other hand, *AXIN2* did not affect luciferase activity driven by a mutated, nonfunctional TCF-binding sites (FOPflash). These data clearly indicate that AXIN2 is involved in the WNT–APC–β-catenin pathway in CRCs.

We have demonstrated preferential transcriptional silencing of *AXIN2* in MSI$^+$ CRCs. Recently, mutations within exon 7 of the *AXIN2* gene have been reported in MSI$^+$ CRC specimens (Liu *et al*., 2000; Wu *et al*., 2001). We have thus analysed the nucleotide sequence of the *AXIN2* gene among our MSI$^+$ samples ($n=9$). Sequencing of the *AXIN2* exon 7 has revealed that only one patient (ID no. 263) carried a mutated *AXIN2* gene in one allele (data not shown). A deletion of a cytosine residue at the nucleotide position 2096 of the *AXIN2* cDNA (GenBank Accession Number, AF078165) led to a frame shift in the open-reading frame in this patient, introducing a premature termination codon in AXIN2 protein at the amino-acid position of 688. However, majority of the patients had intact *AXIN2* genes, indicating that silencing, but not mutation, of *AXIN2* is the main pathway to impede the *AXIN2* function.

The COBRA experiments revealed that the promoter region of *AXIN2* was extensively methylated in MSI$^+$ CRCs but not in MSI$^-$ CRCs. Although the difference in the frequency of *AXIN2* methylation between these two classes of tumor was significant (Fisher's exact probability test, $P=0.003$), the frequency for the MSI$^+$ specimens was still only 29% and therefore was not able to account for all the observed instances of suppression of *AXIN2* expression. We judged COBRA data as positive for methylation if $\geqslant 10\%$ of the PCR products were digested by *Hha*I. However, a small proportion ($<10\%$) of the PCR products was digested in the analysis of $\sim 50\%$ of MSI$^+$ CRC specimens (data not shown), indicating that alterations in the methylation status of the *AXIN2* promoter were more widespread. It is therefore possible that CpG sites other than that targeted by COBRA are more frequently methylated in MSI$^+$ CRCs and are more important for transcriptional regulation.

Similar promoter methylation has been recently described for other genes important for the WNT signaling pathway. The genes for secreted frizzled-related proteins are thus epigenetically silenced in MSI$^+$ CRCs, resulting in constitutive activation of the WNT pathway (Suzuki *et al*., 2004). CpG sites within the *APC* promoter were also found to be frequently methylated in CRCs and other cancers (Esteller *et al*., 2000; Zysman *et al*., 2002). These data thus suggest that not only genetic mutations but also epigenetic silencing might play an important role in tumorigenesis mediated by activation of the WNT pathway.

Methylation of the *APC* promoter in endometrial cancer has been shown to occur preferentially in MSI$^+$ tumors (Zysman *et al*., 2002). Despite the lack of an MSI-associated difference in the expression of *APC* in our CRC specimens (data not shown), the results of this previous study together with our present findings suggest the possibility that genes related to the WNT signaling pathway are targeted for methylation specifically in cancers with MSI. Our data further indicate that such methylation in MSI$^+$ cancers may be directly relevant to the mechanism of malignant transformation through epigenetic silencing of tumor suppressor genes. MSI$^+$ CRCs have been thought to arise through genetic events distinct from those that underlie MSI$^-$ cancers (Rajagopalan and Lengauer, 2004), which are frequently associated with aneuploidy and mutations in WNT pathway genes such as *APC* and *CTNNB1*. However, our data indicate that the molecular mechanisms for malignant transformation overlap between MSI$^+$ and MSI$^-$ CRCs.

Figure 3 Induction of cell death by restoration of *AXIN2* expression in a CRC cell line with a methylated *AXIN2* promoter. (**a**) HCT116 cells were incubated for 72 h with 0, 0.2, or 1 μM 5′-azacytidine and were then subjected to COBRA for determination of the methylation status of the *AXIN2* promoter (Xiong and Laird, 1997). Genomic DNA was denatured, incubated for 16 h at 55°C in 3.1 M sodium bisulfite, and then subjected to PCR with the primers in Figure 2c. The PCR products were then digested with the restriction endonuclease *Hha*I (Takara Bio), and the resulting DNA fragments were fractionated by polyacrylamide gel electrophoresis. The gel was stained with SYBR Green I (Takara Bio) and scanned with an LAS3000 imaging system (Fuji Film). Genomic fragments were determined to be positive for CpG methylation if $\geqslant 10\%$ of the PCR products were cleaved by the restriction endonuclease. Lane M, DNA size markers (50-bp ladder). (**b**) The cells from (**a**) were also subjected to RT–PCR analysis for determination of the amount of *AXIN2* mRNA relative to that of *ACTB* mRNA. (**c**) Cells treated as in (**a**) with 0, 0.2, 1, or 5 μM 5′-azacytidine were examined by light microscopy. Cell death was estimated by counting the remaining viable cells in each culture dish by the dye-exclusion method. Scale bar, 50 μm. (**d**) Human kidney 293 cells infected with either a mock virus or a recombinant virus encoding both MYC epitope-tagged AXIN2 and mouse CD8. A human cDNA for AXIN2 tagged at its NH_2-terminus with the MYC epitope sequence was ligated into the pMX-iresCD8 retroviral plasmid (Yamashita *et al*., 2001) to yield pMX-AXIN2-MYC-iresCD8. The latter plasmid was introduced into BOSC23 cells together with pE-ampho and pGP packaging plasmids (Takara Bio) by transfection with the use of Lipofectamine (Invitrogen). The culture supernatant containing recombinant viruses was added to 293 cells with 4 μg/ml of polybrene (Sigma). Cells were then subjected to immunoprecipitation with the antibodies to MYC (9E10, Roche Diagnostics), and to immunoblot analysis with the same antibodies. (**e**) HCT116 cells infected with the viruses in (**d**) were subjected to affinity chromatography to isolate CD8$^+$ cells, which were then subjected to RT–PCR analysis for quantitation of *AXIN2* mRNA relative to the amount of *ACTB* mRNA. (**f**) The CD8$^+$ fractions in (**e**) were seeded at a density of 5×10^4 cells/dish and cultured for 72 h, after which the ratio of the final cell number to the initial value was determined. Data are means + s.d. of triplicate from a representative experiment. The *P*-value for the indicated comparison was determined by Student's *t* test. (**g**) HCT116 cells were seeded at a density of 2.5×10^6 cells/6 cm dish. After 24 h of incubation, the cells were transfected, with the use of Lipofectamine, with 2 μg of pMX-AXIN2-MYC-iresCD8 (AXIN2) or pMX-iresCD8 (Mock). For the reporter plasmids, 0.5 μg of pGL4 (Promega, Madison, WI, USA) plus either 0.5 μg of pTOPflash or 0.5 μg of pFOPflash (both from Upstate Biotechnology, Lake Placid, NY, USA) were added to the lipofection mix. The activity of *Photinus pyralis* luciferase was measured after 24 h of incubation with the use of the Dual-luciferase reporter assay system (Promega), and normalized on the basis of the activity of *Renilla reniformis* luciferase produced by pGL4. Data are shown as the mean value + s.d. of triplicate samples.

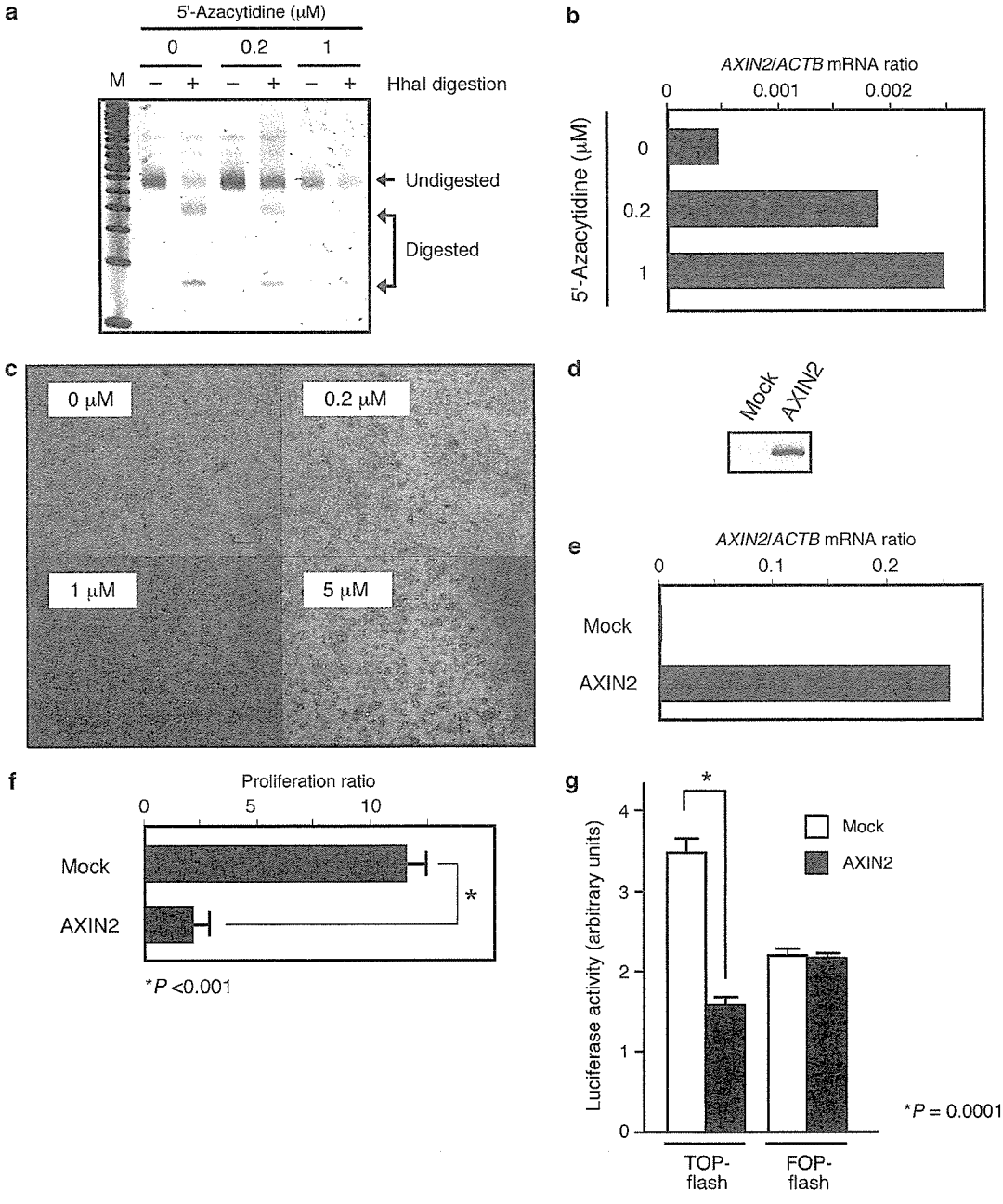

Acknowledgements

We thank M Toyota and SN Thibodeau for critical reading of the manuscript and helpful suggestions. This study was supported in part by a grant for Third-Term Comprehensive Control Research for Cancer from the Ministry of Health, Labor, and Welfare of Japan, and by a grant for 'High-Tech Research Center' Project for Private Universities: Matching Fund Subsidy (2002–2006) from the Ministry of Education, Culture, Sports, Science, and Technology of Japan.

References

Alon U, Barkai N, Notterman DA, Gish K, Ybarra S, Mack D *et al.* (1999). *Proc Natl Acad Sci USA* **96**: 6745–6750.
Behrens J, Jerchow BA, Wurtele M, Grimm J, Asbrand C, Wirtz R *et al.* (1998). *Science* **280**: 596–599.
Boland CR, Thibodeau SN, Hamilton SR, Sidransky D, Eshleman JR, Burt RW *et al.* (1998). *Cancer Res* **58**: 5248–5257.
Bronner CE, Baker SM, Morrison PT, Warren G, Smith LG, Lescoe MK *et al.* (1994). *Nature* **368**: 258–261.

Christman JK. (2002). *Oncogene* **21**: 5483–5495.
Cunningham JM, Christensen ER, Tester DJ, Kim CY, Roche PC, Burgart LJ *et al.* (1998). *Cancer Res* **58**: 3455–3460.
Esteller M, Sparks A, Toyota M, Sanchez-Cespedes M, Capella G, Peinado MA *et al.* (2000). *Cancer Res* **60**: 4366–4371.
Fellenberg K, Hauser NC, Brors B, Neutzner A, Hoheisel JD, Vingron M. (2001). *Proc Natl Acad Sci USA* **98**: 10781–10786.
Fishel R, Lescoe MK, Rao MR, Copeland NG, Jenkins NA, Garber J *et al.* (1993). *Cell* **75**: 1027–1038.
Ionov Y, Peinado MA, Malkhosyan S, Shibata D, Perucho M. (1993). *Nature* **363**: 558–561.
Issa JP. (2004). *Nat Rev Cancer* **4**: 988–993.
Kinzler KW, Vogelstein B. (1996). *Cell* **87**: 159–170.
Koinuma K, Shitoh K, Miyakura Y, Furukawa T, Yamashita Y, Ota J *et al.* (2004). *Int J Cancer* **108**: 237–242.
Korinek V, Barker N, Morin PJ, van Wichen D, de Weger R, Kinzler KW *et al.* (1997). *Science* **275**: 1784–1787.
Lengauer C, Kinzler KW, Vogelstein B. (1998). *Nature* **396**: 643–649.
Leung JY, Kolligs FT, Wu R, Zhai Y, Kuick R, Hanash S *et al.* (2002). *J Biol Chem* **277**: 21657–21665.
Liu W, Dong X, Mai M, Seelan RS, Taniguchi K, Krishnadath KK *et al.* (2000). *Nat Genet* **26**: 146–147.
Miyakura Y, Sugano K, Konishi F, Ichikawa A, Maekawa M, Shitoh K *et al.* (2001). *Gastroenterology* **121**: 1300–1309.
Narayan S, Roy D. (2003). *Mol Cancer* **2**: 41.
Ohki-Kaneda R, Ohashi J, Yamamoto K, Ueno S, Ota J, Choi YL *et al.* (2004). *Biochem Biophys Res Commun* **320**: 1328–1336.
Papadopoulos N, Nicolaides NC, Wei YF, Ruben SM, Carter KC, Rosen CA *et al.* (1994). *Science* **263**: 1625–1629.
Rajagopalan H, Lengauer C. (2004). *Nature* **432**: 338–341.
Rubinfeld B, Robbins P, El-Gamil M, Albert I, Porfiri E, Polakis P. (1997). *Science* **275**: 1790–1792.
Satoh S, Daigo Y, Furukawa Y, Kato T, Miwa N, Nishiwaki T *et al.* (2000). *Nat Genet* **24**: 245–250.
Smith G, Carey FA, Beattie J, Wilkie MJ, Lightfoot TJ, Coxhead J *et al.* (2002). *Proc Natl Acad Sci USA* **99**: 9433–9438.
Suzuki H, Watkins DN, Jair KW, Schuebel KE, Markowitz SD, Dong Chen W *et al.* (2004). *Nat Genet* **36**: 417–422.
Tolwinski NS, Wieschaus E. (2004). *Trends Genet* **20**: 177–181.
Toyota M, Ahuja N, Ohe-Toyota M, Herman JG, Baylin SB, Issa JP. (1999). *Proc Natl Acad Sci USA* **96**: 8681–8686.
Veigl ML, Kasturi L, Olechnowicz J, Ma AH, Lutterbaugh JD, Periyasamy S *et al.* (1998). *Proc Natl Acad Sci U S A* **95**: 8698–8702.
Wheeler JM, Beck NE, Kim HC, Tomlinson IP, Mortensen NJ, Bodmer WF. (1999). *Proc Natl Acad Sci USA* **96**: 10296–10301.
Wu R, Zhai Y, Fearon ER, Cho KR. (2001). *Cancer Res* **61**: 8247–8255.
Xiong Z, Laird PW. (1997). *Nucleic Acids Res* **25**: 2532–2534.
Yamashita Y, Kajigaya S, Yoshida K, Ueno S, Ota J, Ohmine K *et al.* (2001). *J Biol Chem* **276**: 39012–39020.
Zysman M, Saka A, Millar A, Knight J, Chapman W, Bapat B. (2002). *Cancer Res* **62**: 3663–3666.

Supplementary Information accompanies the paper on Oncogene website (http://www.nature.com/onc).

Oncology Research, Vol. 16, pp. 85–95
Printed in the USA.

0965-0407/06 $90.00 + .00
E-ISSN 1555-3906
www.cognizantcommunication.com

Schedule-Dependent Interactions Between Pemetrexed and Cisplatin in Human Carcinoma Cell Lines In Vitro

Yasuhiko Kano,* Miyuki Akutsu,* Saburo Tsunoda,* Tohru Izumi,* Hiroyuki Kobayashi,* Koichi Inoue,† Kiyoshi Mori,‡ Hirofumi Fujii,‡ Hiroyuki Mano,§ Tsogbadrakh Odgerel,¶ and Yusuke Furukawa¶

*Division of Hematology, Tochigi Cancer Center, 4-9-13, Yonan, Utsunomiya, Tochigi, 320-0834, Japan
†Division of Radiation Oncology, Tochigi Cancer Center, 4-9-13, Yonan, Utsunomiya, Tochigi, 320-0834, Japan
‡Division of Medical Oncology, Tochigi Cancer Center, 4-9-13, Yonan, Utsunomiya, Tochigi, 320-0834, Japan
§Division of Functional Genomics, Jichi Medical School, 3311-1, Minamikawachi, Tochigi, 329-0431, Japan
¶Division of Stem Cell Regulation, Jichi Medical School, 3311-1, Minamikawachi, Tochigi, 329-0431, Japan

(Submitted July 1, 2005; revision received December 26, 2005; accepted January 10, 2006)

The combination of pemetrexed and cisplatin shows good clinical activity against mesothelioma and lung cancer. In order to study the potential cellular basis for this, and provide leads as to how to optimize the combination, we studied the schedule-dependent cytotoxic effects of pemetrexed and cisplatin against four human cancer cell lines in vitro. Tumor cells were incubated with pemetrexed and cisplatin for 24 h at various schedules. The combination effects after 5 days were analyzed by the isobologram method. Both simultaneous exposure to pemetrexed and cisplatin for 24 h and sequential exposure to cisplatin for 24 h followed by pemetrexed for 24 h produced antagonistic effects in human lung cancer A549, breast cancer MCF7, and ovarian cancer PA1 cells and additive effects in colon cancer WiDr cells. Pemetrexed for 24 h followed by cisplatin for 24 h produced synergistic effects in MCF7 cells, additive/synergistic effects in A549 and PA1 cells, and additive effects in WiDr cells. Cell cycle analysis of MCF7 and PA1 cells supported these findings. Our results suggest that the simultaneous clinical administration of pemetrexed and cisplatin may be suboptimal. The optimal schedule of pemetrexed in combination with cisplatin at the cellular level is the sequential administration of pemetrexed followed by cisplatin and this schedule is worthy of clinical investigations.

Key words: Pemetrexed; Cisplatin; Isobologram; Synergism; Antagonism

INTRODUCTION

Pemetrexed (multitargeted antifolate) is a novel antifolate that inhibits multiple points in folate metabolism including thymidylate synthase, dihydrofolate reductase, and glycinamide ribonucleotide formyl transferase (1–3). Preclinical studies of pemetrexed have demonstrated antitumor activity against a variety of human cancer cells in preclinical models (4). The optimal dose and schedule of pemetrexed was considered to be 500 mg/m^2 in a 10-min infusion once every 3 weeks (5,6). Clinical trials of pemetrexed showed a broad activity against a variety of solid tumors including malignant mesothelioma, and colorectal, pancreas, lung, head and neck, gastric, bladder, and breast cancers (6–14). Dose-limiting toxicities included neutropenia, mucositis, diarrhea, and severe nausea and vomiting (5,6). Patients with a folate-deficient state were associated with severe toxicity, and folate and cobalamin administration before pemetrexed has been introduced in clinical trials (9,13).

Combination chemotherapy has become a standard in the treatment of cancer, based upon theoretical advantages and on proven clinical efficacy. The clinical studies of pemetrexed and platinums (e.g., cisplatin, carboplatin, and oxaliplatin) in combinations have been used against malignant mesothelioma and non-small cell lung cancer, and the promising activity of this combination has been observed (15–19). The wide range of antitumor activity of pemetrexed and platinums (20), their different cytotoxic mechanisms and different toxic profiles, and the absence of cross-resistance provide a rationale for using combinations of these agents.

The cytotoxic action of cisplatin is considered to be the result of the formation of cisplatin–DNA adducts

Address correspondence to Yasuhiko Kano, Division of Hematology, Tochigi Cancer Center, Yonan 4-9-13, Utsunomiya, Tochigi, 320-0834, Japan. Tel: 011-81-28-658-5151; Fax: 011-81-28-658-5488; E-mail: ykano@tcc.pref.tochigi.jp

(20). Pemetrexed treatment may influence adduct formation by cisplatin or the repair of formed adducts, because pemetrexed inhibits both pyrimidine and purine synthesis. The disturbances of the cell cycle produced by pemetrexed and cisplatin may also influence the cytotoxic effects of each other because these agents are cell cycle specific (21,22).

These suggest that the drug schedule may play a significant role in the outcome, and therefore the design of a protocol using them in combination may requires careful consideration. Schedule-dependent interactions have been observed for the combinations of pemetrexed and gemcitabine (23), doxorubicin (24), or paclitaxel (25) in in vitro studies. Because experimental studies for the combination of pemetrexed with cisplatin are limited (26, 27), the optimal schedule of this combination is obscure.

The present study aimed at elucidating the cytotoxic effects of combinations of pemetrexed and cisplatin in various schedules on four human carcinoma cell lines. Our data suggest that the simultaneous administration of pemetrexed and cisplatin may be suboptimal for this combination and the optimal schedule of this combination at the cellular level is the sequential administration of pemetrexed followed by cisplatin.

MATERIALS AND METHODS

Cell Lines

The human lung cancer A549, the breast cancer MCF7, the ovarian cancer PA1, and the colon cancer WiDr cells were used. These cells were obtained from the American Type Culture Collection (Rockville, MD) and maintained in RPMI-1640 medium (Sigma Chemical Co., St Louis, MO) supplemented with 10% heat-inactivated fetal bovine serum (FBS) (Grand Island Biological Co.) and antibiotics. The doubling times of A549, MCF7, PA1, and WiDr cells in our experimental conditions were 20–24 h.

Drugs

Pemetrexed was kindly provided by Eli Lilly and Company (Indianapolis, IN). Cisplatin was purchased from Nihon Kayaku Co. (Tokyo). Drugs were diluted with RPMI-1640 plus 10% FBS.

Cell Growth Inhibition Using Combined Anticancer Agents

On day 0, cells growing in the exponential phase were harvested with 0.05% trypsin and 0.02% EDTA and resuspended to a final concentration of 5.0×10^3 cells/ml in fresh medium containing 10% FBS and antibiotics. The cell suspensions (100 μl) were dispensed using a multichannel pipette into the individual wells of a 96-well tissue culture plate with a lid (Falcon, Oxnard, CA). Each plate had one 8-well control column containing medium alone and one 8-well control column containing cells without drug. Eight plates were prepared for each drug combination. The cells were preincubated overnight to allow attachment.

Simultaneous Exposure to Pemetrexed and Cisplatin

After 16–20-h incubation for cell attachment, solutions of pemetrexed and cisplatin (50 μl) at different concentrations were added to the individual wells. The plates were also incubated under the same conditions for 24 h. The cells were then washed twice with culture medium containing 1% FBS, and then fresh medium containing 10% FBS (200 μl) and antibiotics was added. The cells were incubated again for 4 days.

Sequential Exposure to Pemetrexed Followed by Cisplatin or Vice Versa

After 16–20-h incubation, medium containing 10% FBS (50 μl) and solutions (50 μl) of pemetrexed (or cisplatin) at different concentrations was added to the individual wells. The plates were then incubated under the same conditions for 24 h. The cells were washed

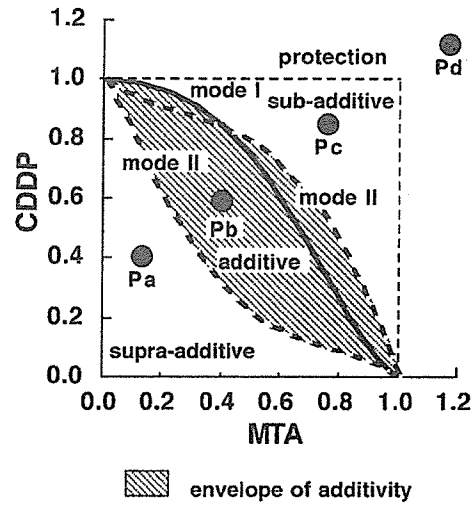

Figure 1. Schematic representation of an isobologram (29). The envelope of additivity, surrounded by mode I (solid line) and mode II (dotted lines) isobologram lines, was constructed from the dose–response curves of pemetrexed (MTA) and cisplatin (CDDP). The concentrations that produced 80% cell growth inhibition were expressed as 1.0 in the ordinate and the abscissa of all isobolograms for MCF7, PA1, and WiDr cells, while the concentrations that produced 50% cell growth inhibition were expressed as 1.0 in the ordinate and the abscissa of all isobolograms for A549 cells. The combined data points Pa, Pb, Pc, and Pd show supra-additive, additive, subadditive, and protective effects, respectively.

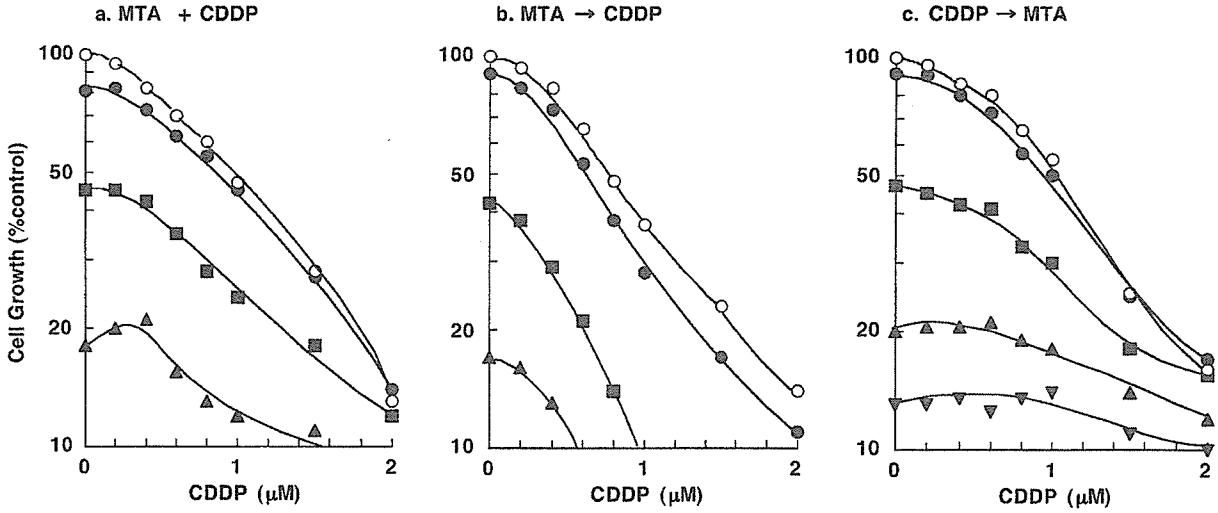

Figure 2. Schedule dependence of the interaction between pemetrexed and cisplatin in PA1 cells. Cells were exposed to these two drugs simultaneously for 24 h (a), pemetrexed first for 24 h followed by cisplatin for 24 h (b), or the reverse sequence (c). The cell number after 5 days was measured using the MTT assay and was plotted as a percentage of the control (cells not exposed to drugs). The concentrations of cisplatin are shown on the abscissa. The concentrations of pemetrexed were 0 (open circles), 20 (filled circles), 50 (filled squares), 100 (filled upward triangles), and 200 (filled downward triangles) nM, respectively. Data are mean values for three independent experiments; SE was <20%.

twice with culture medium containing 1% FBS; fresh medium containing 10% FBS (150 μl) and antibiotics was added, followed by the addition of solutions (50 μl) of cisplatin (or pemetrexed) at different concentrations. The plates were incubated again under the same conditions for 24 h. The cells were then washed twice with culture medium, and fresh medium containing 10% FBS (200 μl) and antibiotics was added. The cells were then incubated again for 3 days.

MTT Assay

The cytotoxicity of pemetrexed alone, cisplatin alone, and their combinations was determined by 3-(4,5-dimethylthiazol-2-yl)-2,5-diphenyltetrazolium bromide (MTT) assay as described previously (28). For all four cell lines examined, we were able to establish a linear relationship between the MTT assay value and the cell number within the range shown.

Isobologram

The dose–response interactions between pemetrexed and cisplatin for the MCF7, PA1, and WiDr cells were evaluated at the IC_{80} level by the isobologram method of Steel and Peckham (Fig. 1) (29). The IC_{80} was defined as the concentration of drug that produced 80% cell growth inhibition (i.e., an 80% reduction in absorbance). Although the drug interaction at IC_{90} or more would be more important than both IC_{80} and IC_{50} for cancer chemotherapy, it is difficult to get reliable data at IC_{90} or more using MTT assay. A549 was resistant to pemetrexed and the interactions between them were evaluated at the IC_{50} level.

We used the isobologram method of Steel and Peckham because this method can cope with any agents with unclear cytotoxic mechanisms and a variety of dose–response curves of anticancer agents. The concept and analysis of the isobologram has been described in detail previously (30,31). The isobologram of Steel and Peckham is very strict for synergism and antagonism.

If the two agents act additively by independent mechanisms, the combined data points would lie near the mode I line (hetero-addition). If the agents act additively by similar mechanisms, the combined data points would lie near the mode II lines (iso-addition). When the data points of the drug combination fell within the area surrounded by mode I and /or mode II lines (i.e., within the envelope of additivity), the combination was described as additive.

A combination that gives data points to the left of the envelope of additivity (i.e., the combined effect is caused by lower doses of the two agents than is predicted) can confidently be described as supra-additive (synergism). A combination that gives data points to the right of the envelope of additivity, but within the square or on the line of the square, can be described as subadditive (i.e., the combination is superior or equal to a single agent but is less than additive). A combination that gives

data points outside the square can be described as protective (i.e., the combination is inferior in cytotoxic action to a single agent). A combination with both subadditive and/or protective interactions can confidently be described as antagonistic.

Data Analysis

The findings were analyzed as described previously (32). When the observed data points from combinations fell mainly in the area of supra-additivity or in the areas of subadditivity and protection, the mean value of the observed data was smaller than that of the predicted minimum data or larger than that of the predicted maximum data, the combinations were considered to have a synergistic or an antagonistic effect, respectively. To determine whether the condition of synergism (or antagonism) truly existed, a Wilcoxon signed-rank test was performed to compare the observed data with the predicted minimum (or maximum) data for an additive effect. Probability values of $p < 0.05$ were considered significant. Because the isobologram of Steel and Peckham is very strict for synergism and antagonism, combinations with $p \geq 0.05$ were defined as having an additive/synergistic (or additive/antagonistic) effect. All statistical analyses were performed using the Stat View 4.01 software program (Abacus Concepts, Berkeley, CA).

Flow Cytometric Analysis

PA1 cells were treated with 0.2 μM pemetrexed alone or 0.5 μM cisplatin alone or their combination simultaneously for 24 h. MCF7 cells were treated with 0.5 μM pemetrexed alone or 5 μM cisplatin alone or their combination simultaneously for 24 h. The cells were also treated with pemetrexed for 24 h followed by cisplatin for 24 h or the reverse sequence. The cells were harvested at 48 h and the cell cycle profiles were analyzed by staining the intracellular DNA with propidium iodide in preparation for flow cytometry with the FACScan CellFIT system (Becton-Dickinson, San Jose, CA). A DNA histogram was obtained by analyzing 25,000 cells with the ModFIT program (Becton-Dickinson) (33).

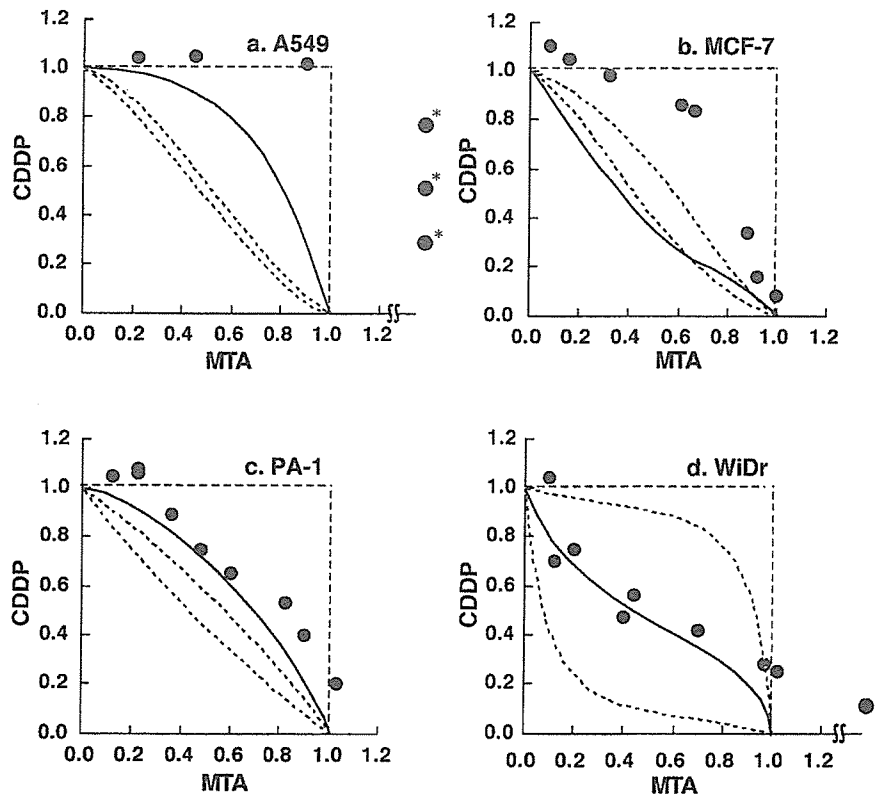

Figure 3. Isobolograms of simultaneous exposure to pemetrexed and cisplatin for 24 h in A549 (a), MCF7 (b), PA1 (c), and WiDr (d) cells. For the A549, MCF7, and PA1 cells, the combined data points fell in the areas of subadditivity and protection. For the WiDr cells, the combined data points fell mainly within the envelope of additivity. Data are mean values for at least three independent experiments; SE was <25% (*except the data).

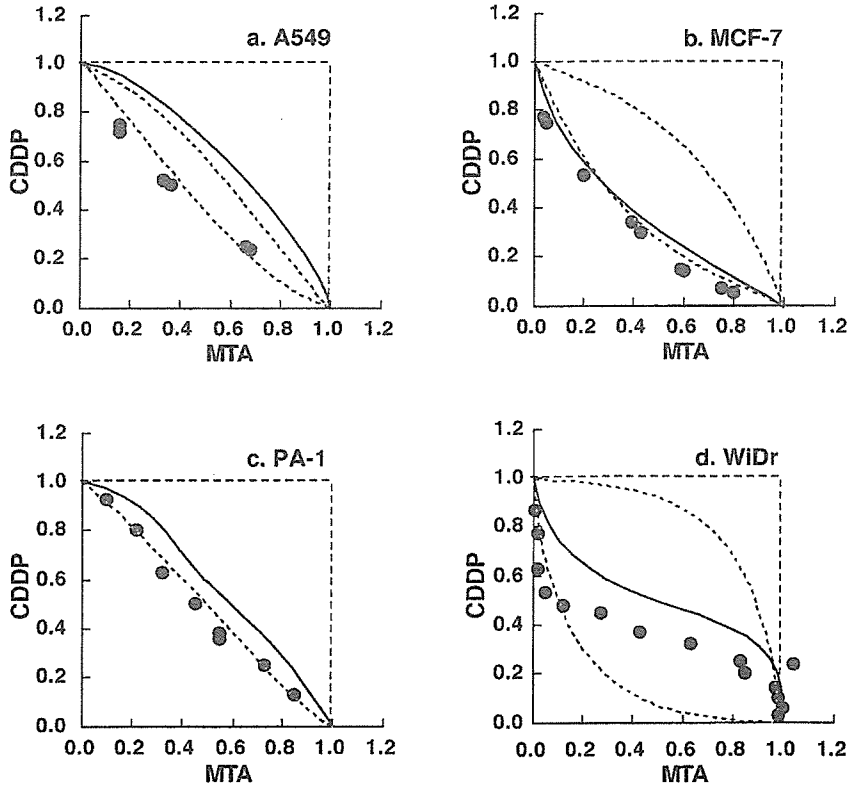

Figure 4. Isobolograms of sequential exposure to pemetrexed (24 h) followed by cisplatin (24 h) in A549 (a), MCF7 (b), PA1 (c), and WiDr (d) cells. For the A549, MCF7, and PA1 cells, all or most of the data points of the combinations fell within the envelope of additivity and in the area of supra-additivity. For the WiDr cells, most of the data points fell within the envelope of additivity. Data are mean values for at least three independent experiments; SE was <20%.

RESULTS

The IC_{80} values of 24-h exposure to pemetrexed for A549, MCF7, PA1, and WiDr cells were >5, 2.5 ± 0.4, 0.10 ± 0.03, and 0.55 ± 0.2 μM, respectively. Because A549 cells were resistant to pemetrexed and the IC_{80} level was not obtained, the interactions between pemetrexed and cisplatin were evaluated at the IC_{50} level. The IC_{50} value of 24-h exposure to pemetrexed for A549 cells was 2.7 ± 0.3 μM.

Figure 2 shows the dose–response curves obtained from simultaneous exposure and sequential exposure to pemetrexed and cisplatin for the PA1 cells. The dose–response curves were plotted on a semilog scale as a percentage of the control, the cell number of which was obtained from the samples not exposed to the drugs administered simultaneously. Dose–response curves in which the pemetrexed concentrations are shown on the abscissa could be made based on the same data (figure not shown). Based upon the dose–response curves of pemetrexed alone and cisplatin alone, three isoeffect curves (mode I and mode II lines) were constructed. Isobolograms at the IC_{80} or IC_{50} levels were generated based upon these dose–response curves for the combinations.

Simultaneous Exposure to Pemetrexed and Cisplatin

Figure 3 shows isobolograms of the A549, MCF7, PA1, and WiDr cells after simultaneous exposure to pemetrexed and cisplatin for 24 h. For the A549, MCF7, and PA1 cells, the combined data points fell in the areas of subadditivity and protection, respectively. The mean values of the observed data (>1.15, 0.95, and 0.69) were larger than those of the predicted maximum values (0.75, 0.72, and 0.56). The observed data and the predicted maximum data were compared by the Wilcoxon signed-rank test. The differences were significant ($p < 0.05$, $p < 0.02$, and $p < 0.01$), indicating antagonistic effects (Table 1). For the WiDr cells, the combined data points fell mainly within the envelope of additivity. The mean values of the observed data (0.66) were larger than those of the predicted minimum values (0.27), and smaller than those of the predicted maximum values (0.73), indicating additive effects.

Sequential Exposure to Pemetrexed Followed by Cisplatin

Figure 4 shows isobolograms of the A549, MCF7, PA1, and WiDr cells exposed first to pemetrexed for 24 h and then cisplatin for 24 h. For the MCF7 cells, combined data points fell in the area of supra-additivity. The mean values of the observed data (0.40) were smaller than those of the predicted minimum values (0.44) (Table 1). The difference between them was significant ($p < 0.01$), indicating synergistic effects. For the A549 and PA1 cells, combined data points fell in the area of supra-additivity and within the envelope of additivity. The mean values of the observed data were smaller than those of the predicted minimum values (Table 1), but the differences were not significant ($p > 0.05$ and $p > 0.05$), indicating additive/synergistic effects. For the WiDr cells, the combined data points fell within the envelope of additivity and in the areas of supra-additivity and protection. The mean value of the observed data was smaller than the predicted maximum values and larger than that of the predicted minimum values (Table 1), indicating additive effects.

Sequential Exposure to Cisplatin Followed by Pemetrexed

Figure 5 shows isobolograms of the four cell lines exposed first to cisplatin for 24 h and then pemetrexed for 24 h. For the A549, MCF7, and PA1 cells, all or most of the combined data points fell in the areas of subadditivity and protection. The mean values of the observed data were larger than those of the predicted maximum values (Table 1). The differences were significant ($p < 0.05$, $p < 0.02$, and $p < 0.02$, respectively), indicating antagonistic effects. For the WiDr cells, most of the combined data points fell within the envelope of additivity, indicating an additive effect of this schedule.

Flow Cytometric Analysis

Finally, we evaluated the cytotoxic effects of pemetrexed and cisplatin on cancer cells using flow cytome-

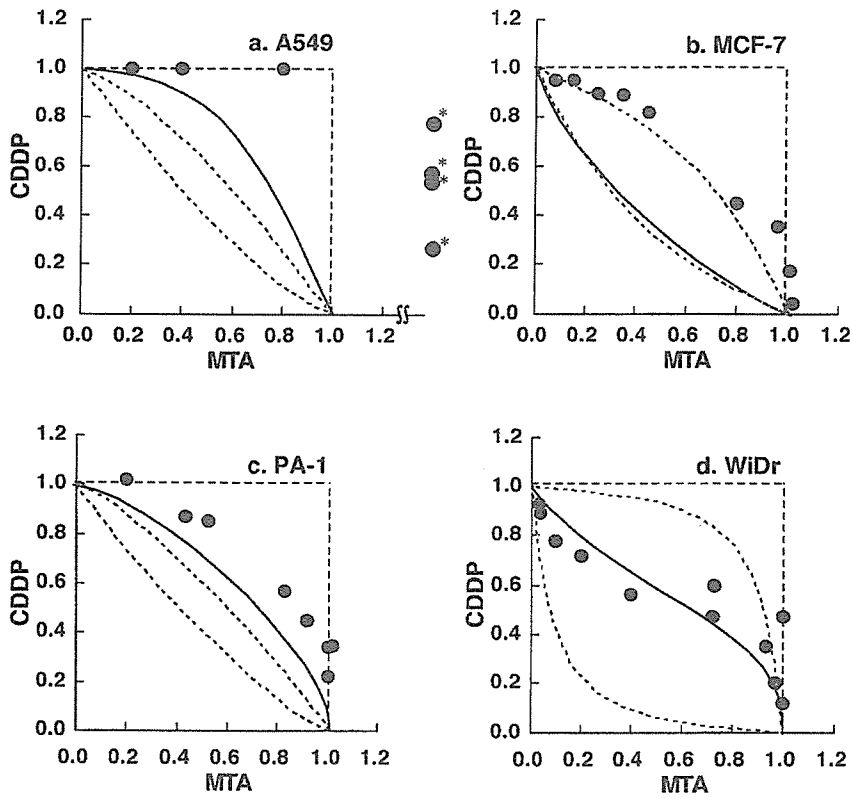

Figure 5. Isobolograms of sequential exposure to cisplatin (24 h) followed by pemetrexed (24 h) in A549 (a), MCF7 (b), PA1 (c), and WiDr (d) cells. For the A549, MCF7, and PA1 cells, all or most of the data points of the combinations fell in the areas of subadditivity and protection. For the WiDr cells, most of the data points of the combinations fell within the envelope of additivity and in the area of subadditivity. Data are mean values for at least three independent experiments; SE was <20%(*except the data).

Table 1. Mean Values of Observed, Predicted Minimum, and Predicted Maximum Data of Pemetrexed (MTA) in Combination With Cisplatin (CDDP) at IC_{80} for MCF7, PA1, and WiDr Cells and at IC_{50} for A549 Cells

Schedule	Cell Line	n	Observed Data	Predictaed Data for an Additive Effect		Effect
				Minimum	Maximum	
MTA + CDDP	A549	6	1.15	0.44	0.75	antagonism ($p < 0.05$)
	MCF7	8	0.95	0.57	0.72	antagonism ($p < 0.02$)
	PA1	9	0.69	0.40	0.56	antagonism ($p < 0.01$)
	WiDr	9	0.66	0.27	0.73	additive
MTA → CDDP	A549+	6	0.45	0.47	0.72	additive/synergism ($p > 0.05$)
	MCF7	9	0.40	0.44	0.78	synergism ($p < 0.01$)
	PA1	8	0.52	0.55	0.64	additive/synergism($p > 0.05$)
	WiDr	15	0.64	0.46	0.84	additive
CDDP → MTA	A549	7	1.14	0.41	0.74	antagonism ($p < 0.05$)
	MCF7	9	0.82	0.52	0.73	antagonism ($p < 0.02$)
	PA1	8	0.75	0.41	0.63	antagonism ($p < 0.02$)
	WiDr	11	0.71	0.21	0.82	additive

try. Cell cycle analysis revealed that pemetrexed and cisplatin arrested PA1 cells in late G_1 to early S phase and G_2/M phase, respectively (Fig. 6A, Table 2). When PA1 cells were exposed to both drugs simultaneously, the cell cycle profile was almost identical to that of a single treatment with pemetrexed, suggesting that the cell cycle effect of pemetrexed is dominant over that of cisplatin. As a result, the apoptosis-inducing effect of cisplatin, which was estimated by an increase in the size of sub-G_1 fraction, was almost completely cancelled in the presence of pemetrexed (Fig. 6A, MTA + CDDP). When PA1 cells were treated with cisplatin first and followed by pemetrexed, the cell cycle pattern closely resembled that of cells treated with cisplatin alone except for a modest increase in G_1 and S phases (Fig. 6A, Table 2, CDDP to MTA). The induction of apoptotsis was less prominent in the CDDP to MTA treatment than in the CDDP treatment (Table 2). In contrast, both apoptosis and G_2/M arrest were enhanced when PA1 cells were treated with pemetrexed first and followed by cisplatin compared with the treatment with either pemetrexed or cisplatin alone (Fig. 6A, Table 2, MTA to CDDP).

We carried out the same analysis with another cancer cell line MCF7 and obtained highly reproducible results. Upon simultaneous addition, the cell cycle effect of cisplatin was almost completely abrogated and the percentage of apoptotic cells was less than that of a single treatment with pemetrexed (Fig. 6B, MTA + CDDP). Similarly, apoptosis was suppressed when MCF7 cells were treated with cisplatin first and followed by pemetrexed compared with the treatment with either pemetrexed or cisplatin alone (Fig. 6B, Table 2, CDDP to MTA). In contrast, the apoptosis-inducing effect of pemetrexed was enhanced by the sequential exposure to cisplatin after pemetrexed (Fig. 6B, Table 2, MTA to CDDP). Overall, these data are fully consistent with the results of isobologram analysis, and provide the molecular basis of the interaction between the two drugs.

DISCUSSION

We found that the cytotoxic interaction between pemetrexed and cisplatin was schedule dependent. Simultaneous exposure to pemetrexed and cisplatin and sequential exposure to cisplatin followed by pemetrexed showed antagonistic effects in A549, MCF7, and PA1 cells, while sequential exposure to pemetrexed followed by cisplatin had a tendency to produce synergistic effects. In the latter schedule, observed data points in A549, MCF7, and PA1 cells were smaller than predicted minimum values for an additive effect (Table 1). WiDr cells showed additive effects in all schedules. The cause of difference in combined effects among cell lines is unknown. The difference may reflect the folate metabolism and the variety of target numbers (enzymes) in the cells. In addition, the isobologram of Steel and Peckham is stricter for synergism and antagonism than other methods. This may also influence the results.

In general, it is difficult to clarify the mechanisms underlying the drug combination. In this study, however, cell cycle analysis provided a clue to understand the molecular basis of schedule-dependent synergism and antagonism of the combination of pemetrexed and cisplatin. The exposure of PA1 and MCF7 cells to pemetrexed for 24 h led to a synchronization of most cells in late G_1 to

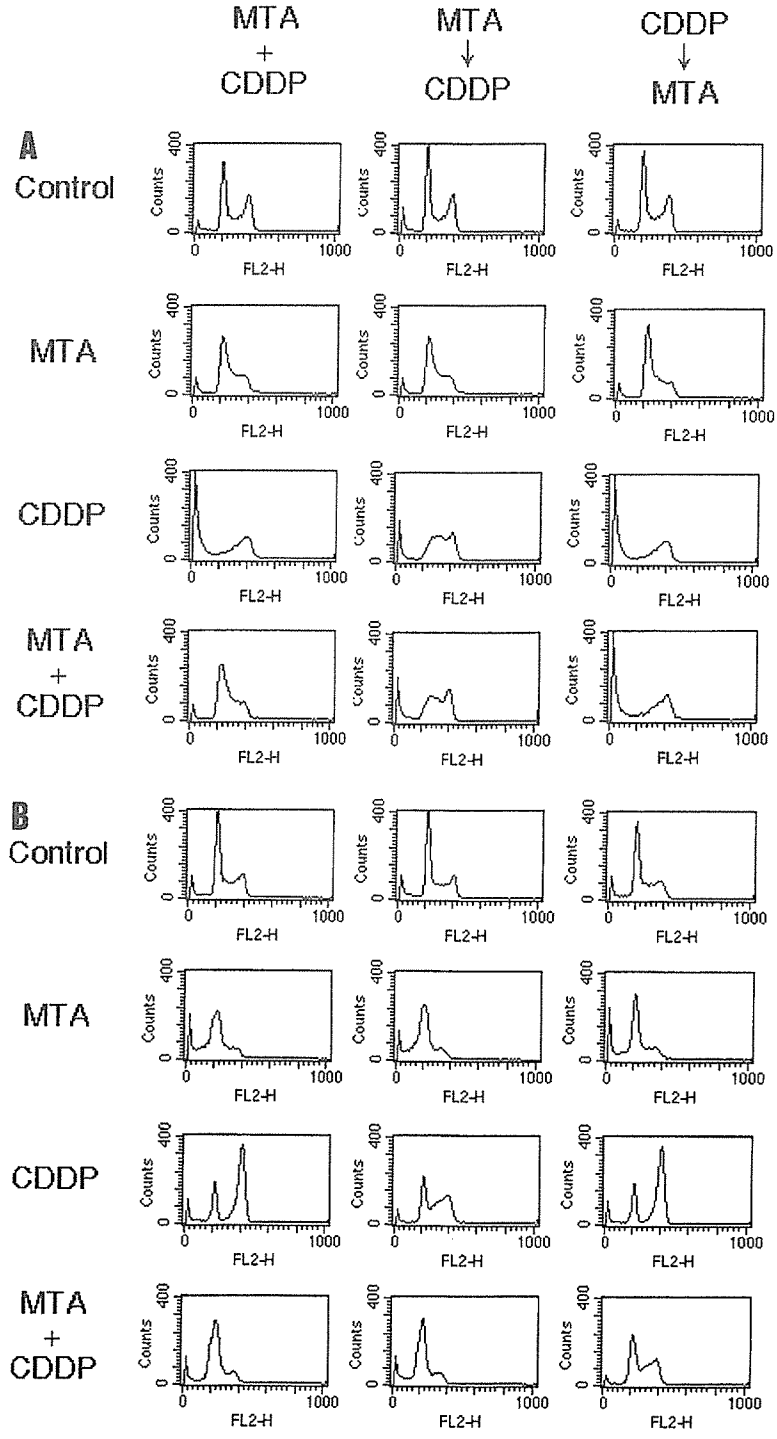

Figure 6. Flow cytometric analysis of cell cycle perturbation. PA1 cells, treated with 0.2 μM pemetrexed (MTA), 0.5 μM cisplatin (CDDP), both drugs simultaneously for 24 h, pemetrexed for 24 h followed by cisplatin for 24 h, or the reverse sequence were harvested at 48 h (A), and MCF7 cells, treated with 0.5 μM pemetrexed (MTA), 5 μM cisplatin (CDDP), both drugs simultaneously for 24 h, pemetrexed for 24 h followed by cisplatin for 24 h, or the reverse sequence were harvested at 48 h (B) and stained for DNA with propidium iodide and analyzed by flow cytometry as described in Materials and Methods.

Table 2. Cell Cycle Perturbations Induced by Pemetrexed (MTA), Cisplatin (CDDP), and Their Combinations for PA1 and MCF7 Cells at 48 h

	MTA + CDDP (24 h)				MTA (24 h) → CDDP (24 h)				CDDP (24 h)→ MTA (24 h)			
Cell Cycle (%)	Control	MTA	CDDP	MTA + CDDP	Control	MTA	CDDP	MTA + CDDP	Control	MTA	CDDP	MTA + CDDP
PA1 cells												
Sub-G_1	3.6	2.4	42.9	2.1	4.3	3.1	8.9	15.3	2.9	2.2	45.1	41.8
G_1	56.2	64.1	7.3	67.1	58.1	65.3	5.8	4.4	57.3	60.1	6.9	10.6
S	15.6	26.7	17.2	19.1	10.4	25.9	48.4	38.7	11.0	30.4	15.8	20.1
G_2/M	24.6	6.8	19.1	11.7	27.2	5.7	36.9	41.6	28.8	7.3	32.2	27.5
MCF-7 cells												
Sub-G_1	4.2	17.5	3.9	5.8	5.3	11.1	2.9	16.8	5.1	10.3	3.6	2.5
G_1	57.6	53.4	28.8	63.7	55.8	61.3	22.3	60.6	58.8	57.2	27.9	25.8
S	16.8	26.9	4.7	21.4	19.1	22.1	21.2	13.8	16.4	28.6	5.0	20.4
G_2/M	21.4	2.2	62.6	9.1	25.1	5.5	53.6	8.8	19.7	3.9	63.5	51.3

early S phase, in which cells are sensitive to cisplatin (20). This may explain the synergistic effects of sequential exposure to pemetrexed followed by cisplatin. On the contrary, one agent may reduce the cytotoxicity of the other agent by preventing cells from entering the specific phase in which the cells are most cytotoxic to the other agent. It has been shown that cisplatin elicits cytotoxic effects by blocking cells in G_2/M phase (20), while pemetrexed does by blocking cells in S phase (21). Indeed, simultaneous exposure to pemetrexed and cisplatin produced antagonistic effects, which were caused by the cancellation of cisplatin-induced G_2/M arrest by coexisting pemetrexed in PA1 and MCF7 cells. This was also the case with sequential exposure with cisplatin first followed by pemetrexed.

Our findings suggest that the sequential administration of pemetrexed followed by cisplatin may be the optimal schedule for these combinations. For example, administrations of pemetrexed on day 1 and cisplatin on day 2 would be worthy of clinical investigations. The simultaneous administration of pemetrexed and cisplatin and the sequential administration of cisplatin followed by pemetrexed may be inadequate. However, it must be noted that there are a number of difficulties in the translation of results from in vitro models to clinical therapy. The drug metabolism and pharmacokinetics under in vivo and in vitro conditions are different. Clinical outcome includes both the antitumor effects and normal tissue toxicity that results from a variable drug exposure, whereas in vitro models represent only antitumor effects at a constant drug exposure.

Teicher et al. studied the combination of pemetrexed with cisplatin in vivo against EMT-6 murine mammary carcinoma by a tumor cell survival assay (26). They observed that pemetrexed administered four times over 48 h with cisplatin administered with the third dose of pemetrexed produced an additive or more than additive tumor response. Teicher et al. further studied the combination of pemetrexed with cisplatin in human tumor xenografts (27). Administration of pemetrexed (days 7–11, days 14–18) along with cisplatin (day 7) produced greater-than-additive effects for human lung cancer H460 and Calu-6 tumor growth delay. Because experimental systems, schedules of drug administrations, and evaluating methods for synergism are different, it is difficult to compare their findings and ours.

A clinical and pharmacokinetic phase I study of pemetrexed in combination with cisplatin has been reported by Thordtmann et al. (15). They observed that this combination was clinically active and simultaneous administration of both agents on day on 1 (pemetrexed intravenously over 10 min and cisplatin over 2 h) every 21 days was less toxic than a sequential administration of pemetrexed on day 1 and cisplatin on day 2. They recommended the simultaneous administration of pemetrexed at 500 mg/m^2 plus cisplatin at 75 mg/m^2 on day 1 every 21 days for this combination. Phase II and III studies of the same schedules have been started for this combination and encouraging results have been obtained so far (16–18).

Our in vitro findings are not contradictory to clinical findings. In our study, simultaneous exposure to pemetrexed and cisplatin produced additive effects in WiDr cells and antagonistic effects in A549, MCF7, andPA1 cells. Most data points fell in the area of sudadditivity in MCF7 and PA1 cells, suggesting that the combination is superior to each drug alone but "sub-optimal." The simultaneous administration of pemetrexed and cisplatin was less toxic than the sequential administration, probably due to antagonistic interaction in the simultaneous exposure. Our isobologram shows that the doses of both agents in the pemetrexed–cisplatin sequence required